

Surface-Induced Deprotection of THP-Protected Hydroxamic Acids on Titanium Dioxide

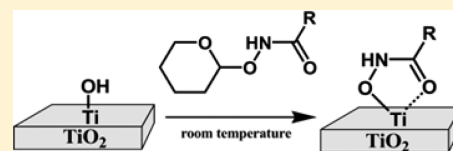
Bradley J. Brennan,^{§,†} Christopher Koenigsmann,^{§,‡} Kelly L. Materna,[†] Paul M. Kim,[†] Matthieu Koepf,[†] Robert H. Crabtree,[†] Charles A. Schmuttenmaer,[†] and Gary W. Brudvig^{*,†}

[†]Energy Sciences Institute and Department of Chemistry, Yale University, P.O. Box 208107, New Haven, Connecticut 06520-8107, United States

[‡]Department of Chemistry, Fordham University, 441 East Fordham Road, Bronx, New York 10458, United States

S Supporting Information

ABSTRACT: Hydroxamic acids chelate metals with high affinity and form hydrolytically stable complexes with metal oxides such as TiO₂. However, these appealing binding properties can cause problems during the preparation and application of metallocatalysts with appended hydroxamate anchoring groups. Here we show that the tetrahydropyran (THP) O-protected hydroxamate group can be cleaved in situ on a TiO₂ surface at room temperature, leading to the surface-bound species. Surface-mediated deprotection has several advantages over direct surface functionalization including increased hydrolytic stability of the covalent interaction with the metal oxide surface and decreased aggregation of the surface species. Application of the surface-mediated chelation method for dye-sensitized photoelectrochemical cells (DSPEC) was examined using the organic dye MK-2. Results show that the surface-mediated deprotection led to improved DSPEC performance attributed to a decrease in dye aggregation relative to a DSPEC prepared using standard methods. This simplified approach using THP-protected hydroxamates provides a convenient new method for functionalizing metal oxides.



1. INTRODUCTION

Functional materials consisting of molecular monolayers on metal oxides are key components in a wide variety of research areas including photoelectrochemical cells, analytical and preparative chromatography techniques, and biological imaging.^{1–6} Methods for functionalizing metal oxides have recently expanded with the introduction of additional anchoring groups such as silatranes and hydroxamic acids.^{7–13} These provide increased stability of the covalent interaction with the surface toward hydrolysis or under device irradiation conditions when compared with carboxylic acid and phosphonic acid functional groups on common metal oxide substrates such as TiO₂.^{12,14,15} Hydrolytic stability is vital when working in aqueous conditions, especially at alkaline pH, and in solutions where traces of water can induce leaching of the chemisorbed monolayer. For this reason, there is increasing interest in the use of silatranes and hydroxamic acids as surface-anchoring functional groups in molecular designs for aqueous-based photoelectrochemical cells.^{12,13}

We have previously shown that hydroxamic acids are a suitable replacement for carboxylic acids in photoelectrochemical cells due to their superior hydrolytic stability and electronic properties that promote rapid photoinduced electron transfer between the monolayer and metal oxide conduction band.^{7,8,11} Their straightforward synthesis from carboxylic acids and hydroxylamine derivatives allows for integration into molecular designs that would have otherwise utilized a less stable carboxylate surface anchor.¹² The use of the *O*-tetrahydro-2*H*-pyran-2-yl (THP) protected form increases resistance to

metal chelation, providing a route to synthesize catalysts with appended THP-protected hydroxamates.

We have recently begun analyzing the hydroxamic acid (HA) moiety in detail, particularly focusing on how it binds to metal oxides.¹⁶ When we attempted deposition from the THP-protected form, we observed spontaneous deprotection at room temperature on a variety of metal oxides including silica, tin oxide, and titanium dioxide to form a functionalized substrate.¹² Similar reactions have been utilized for deprotection of THP-protected alcohols on acidic heterogeneous substrates, albeit without any strong adhesion to the material.¹⁷ The surface deprotection route is similar in principle to the one that applies to the silatrane functional group, where a trialkoxysilane protected with triethanolamine is deprotected on metal oxide surfaces to form siloxyl monolayers.¹⁴ Here, we report a detailed analysis of the surface-mediated deprotection of THP-protected hydroxamic acids on anatase TiO₂, leading to the surface-bound species. We employ infrared spectroscopy to characterize the binding mode of the hydroxamate bound species, dye desorption experiments to characterize the relative binding strength, and nanosecond transient absorption measurements to characterize the rate of interfacial electron transfer. In addition, we also explore the performance of the surface-bound dyes with hydroxamic acid anchoring groups in photoelectrochemical cells as a function of the method of surface binding.

Received: March 14, 2016

Revised: May 13, 2016

Published: May 18, 2016

2. EXPERIMENTAL METHODS

2.1. Materials. *O*-(Tetrahydro-2*H*-pyran-2-yl)-hydroxylamine and TiO₂ powder (anatase, <25 nm particle size) were obtained from Aldrich, phenylhydroxamic acid (phenyl-HA) was obtained from TCI Chemicals, acetohydroxamic acid (aceto-HA) was obtained from Acros, and tetrahydro-2*H*-pyran-2-ol (THP-OH) was obtained from Santa Cruz Biotech. MK-2THP and MK-2HA were prepared according to a published procedure.¹² Other chemicals were obtained from commercial sources and used as received. Fluorine-doped tin oxide (FTO, TEC7 & TEC15) was obtained from Hartford Glass. Titanium dioxide paste was obtained from Solaronix (14411, T-SP) and Dyesol (18NR-AO).

2.2. Synthesis. Aceto-THP: *O*-(Tetrahydro-2*H*-pyran-2-yl)hydroxylamine (127 mg, 1.1 mmol), 4 mL of dry dichloromethane, and 300 μL of triethylamine (2.2 mmol) were added to a dry flask. Acetic anhydride (105 μL, 1.1 mmol) was added, the reaction was refluxed under a nitrogen atmosphere for 4 h, and then it was stirred overnight at room temperature. The solvents were removed by distillation under reduced pressure. The crude material was purified by silica gel column chromatography using deactivated silica prepared by soaking silica in a dichloromethane solution containing 1% triethylamine for 24 h followed by solvent removal. Chromatography was performed using dichloromethane containing 15% acetone as eluent. Fractions containing the pure product were combined and dried by distillation under reduced pressure to yield aceto-HA-THP as a clear viscous gel that converted to a glassy solid over time. Yield: 164 mg (95%).

¹H NMR (400 MHz, methanol-*d*₄): δ 4.88 (t, *J* = 2.4 Hz, 1H, O-CH-O), 3.98 (dt, *J* = 10.8 Hz, 2.6 Hz, 1H, O-CH₂), 3.52–3.57 (m, 1H, O-CH₂), 1.88 (s, 3H, CH₃), 1.84–1.53 (m, 6H). ¹³C NMR (100 MHz, methanol-*d*₄): δ 169.74 (C=O), 103.14 (O-CH-O), 62.99 (O-CH₂), 28.92 (CH₂), 26.24 (CH₂), 19.52, 19.43. Elemental Analysis for C₇H₁₃NO₃: Calculated: C 52.82; H 8.23; N 8.80. Measured: C 53.08; H 8.28; N 8.56.

Phenyl-THP: Benzoic acid (251 mg, 2.05 mmol) and anhydrous benzene (50 mL) were added to a dry flask under nitrogen and were gently stirred at room temperature. Oxalyl chloride (0.21 mL, 2.43 mmol) and anhydrous dimethylformamide (5 μL) were added to the solution. Bubbles in the clear, colorless solution were observed after this addition. After 90 min, approximately 60% of the solvent volume was removed via vacuum. Anhydrous triethylamine (0.28 mL, 2.00 mmol) was added to the clear, yellow solution, which immediately began fuming and turned golden yellow. *O*-(Tetrahydro-pyran-4-yl)-hydroxylamine (358 mg, 3.05 mmol) dissolved in dichloromethane (16 mL) was then added to the solution. The reaction solution was stirred at room temperature for 2 h. Ethyl acetate (50 mL) was added to the solution and then washed with aqueous 5% sodium bicarbonate (2 × 50 mL). The ethyl acetate layer was then washed with brine (50 mL) and dried over sodium sulfate, and the solvent was removed under vacuum producing a white solid. The solid was purified on a silica gel column using a 10% acetone/dichloromethane mixture as the eluent. Fractions containing the pure product were combined and dried under vacuum. The product was a white solid. Yield: 213 mg (47%).

¹H NMR (400 MHz, acetone-*d*₆) δ 10.75 (s, 1H, NH), 7.87–7.79 (m, 2H, aryl-H), 7.57–7.50 (m, 1H, aryl-H), 7.49–7.39 (m, 2H, aryl-H), 5.09 (t, *J* = 2.9 Hz, 1H, CH THP ring), 4.08 (ddd, *J* = 11.5, 9.9, 3.1 Hz, 1H, O-CH-O), 3.53 (dtd, *J* = 11.4, 3.8, 1.6 Hz, 1H, O-CH₂), 1.88–1.68 (m, 3H, O-CH₂-CH₂), 1.67–1.47 (m, 3H, CH₂-CH₂). ¹³C NMR (100 MHz, acetone) δ 205.32 (C=O), 132.92 (C), 131.46 (CH), 128.35 (CH), 127.18 (CH), 101.48 (O-CH-O), 61.46 (CH₂-O), 28.04 (CH₂), 25.06 (CH₂), 18.37 (CH₂). Elemental Analysis for C₁₂H₁₃NO₃: Calculated: C 65.14; H 6.83; N 6.33. Measured: C 64.84; H 6.56; N 6.30.

2.3. Instrumentation. NMR spectra were obtained on a 400 MHz (¹H)/100 MHz (¹³C) instrument, with chemical shifts reported as δ ppm from an internal TMS standard. NMR spectra can be found in the [Supporting Information](#). Elemental analysis was performed by Robertson Microлит Laboratories (Ledgewood, NJ). Nanosecond transient absorption measurements were performed with an LP920 laser flash photolysis spectrometer (Edinburgh Instruments), and the details of these experiments can be found in the [Supporting Information](#). Infrared (IR) spectra were obtained using an Agilent Cary 660 FTIR with a diamond ATR attachment from Pike Technologies. IR spectra of functionalized TiO₂ on FTO were obtained by pressing the substrate onto the ATR diamond surface. Background IR spectra were taken of nonfunctionalized TiO₂ substrates. IR spectra of nonadsorbed compounds were obtained using IR-ATR from dropcast films of the pure materials.

Nanoparticulate titania films (~5 μm) on FTO (TEC15) were prepared using TiO₂ nanoparticle colloid (Solaronix, T/SP) by doctor blading and sintering at 470 °C for a period of 30 min. The electrodes were stored at 110 °C. Functionalization was performed by soaking overnight in ~1 mM solutions of the desired molecule in acetonitrile or toluene and then rinsing in solvent and drying under vacuum. Not all molecules were entirely soluble in toluene at this concentration. However, the spectra obtained for toluene and acetonitrile were indistinguishable, with toluene providing higher signal-to-noise.

2.4. Assembly and Characterization of Dye-Sensitized Photoelectrochemical Cell (DSPCs). DSPC cells were assembled according to a previously published procedure, and specific details can be found in the [Supporting Information](#).^{12,18,19} The *J*-*V* characteristics of the functioning devices were measured under illumination by AM1.5G light produced by a 300 W Xe lamp passed through an AM1.5G filter (Newport Corporation) and a Keithley 2400C source meter. The light intensity was adjusted with a diode calibrated by Newport to ASTM E948-09 and E1021-06 standards. The samples were allowed to equilibrate under illumination for a period of 3 min before the *J*-*V* curves were obtained. EQE spectra were collected from the devices by passing the output of a 300 W Xe lamp through a monochromator (Newport Corporation) to select wavelengths from 300–800 nm. Five DSPCs for each molecule were used for statistical averaging.

2.5. Loading Studies Procedure. The loading of phenyl-HA and phenyl-THP on dispersed TiO₂ nanoparticles (Sigma-Aldrich, < 25 nm) was determined by UV-visible spectroscopy. A stock solution of each sensitizer was prepared in anhydrous acetonitrile with a concentration of ~0.3 mM, and the precise concentration was determined by UV-visible spectroscopy. A premeasured quantity of as-received TiO₂ nanoparticle powder (Sigma-Aldrich, 99.7%, 45–55 m²·g⁻¹, Lot: MKBK2771 V) was heated to 120 °C in a drying oven for a period of 24 h before

adding an aliquot of sensitizer solution. The mixture was sonicated for 15 min to disperse the nanoparticles and stirred for 16 h to allow for sensitization. The particles were removed from the solution by centrifugation, and the concentration of the sensitizer was determined in the supernatant by UV–visible spectroscopy, allowing the quantity of sensitizer loaded to be calculated. The number of dye molecules was normalized to the surface area of the particles, which was calculated from the specific surface area of the particles.

2.6. Dye Desorption Experiments. Dye desorption was performed on mesoporous films sensitized with either MK-2THP or MK-2HA for a period of 16 h. After sensitization, the films were removed from the sensitizer solution and placed into anhydrous toluene for a period of 5–10 min to remove excess dye from the pores of the film. The films were then dried under a stream of nitrogen and transferred to a solution of 1% water dissolved in anhydrous dimethylformamide (DMF, Sigma-Aldrich, <0.005% H₂O, 99.8%, stored under argon). Once immersed, the UV–visible spectrum of the solution was measured periodically to detect the evolution of the desorbed dye in the solution. After 160 min, the film was removed from the DMF solution and washed in fresh anhydrous DMF to remove excess dissolved dye from the pores. The film still containing some dye on the surface was then transferred to a solution of ~3 mM tetrabutylammonium hydroxide (TBAH) prepared by diluting a 1 M solution of TBAH (Acros Organics) in methanol in tetrahydrofuran (THF), which removed the remaining dye. The concentration of dye in the TBAH/THF solution was determined by UV–visible spectroscopy. The total dye loading was determined from the sum of the dye desorbed into the H₂O/DMF solution and the dye desorbed into the TBAH/THF solution. The percent dye desorbed shown in Figure 3A was calculated from the amount of dye desorbed at a given time in the H₂O/DMF solution relative to the total amount of dye desorbed.

3. RESULTS AND DISCUSSION

The aceto-, phenyl-, and MK-2THP derivatives shown in Figure 1 were synthesized by coupling activated carboxyl groups with THP-protected hydroxylamine. MK-2HA was obtained from the hydrolytic cleavage of MK-2THP in the presence of acetic acid.

Deprotection of the THP-hydroxamates on the surface of a metal oxide in situ avoids the tedious deprotection step in the

standard synthetic sequence. In addition, THP-protected hydroxamates have greatly improved solubility in organic solvents compared to the deprotected acids. Our previous results suggested that Lewis acidic metals such as Ti(IV), Si(IV), and Sn(IV) could act as catalysts for the acid-promoted deprotection of THP-hydroxamates to hydroxamic acids, with the active catalyst as either the Lewis acid itself or possibly a Brønsted acid originating from the strongly bound surface water monolayer on those metal oxide surfaces.¹²

Initial studies of the deprotection of phenyl-THP on TiO₂ sought to optimize the experimental methods for surface deprotection based on the loading of the surface species and the binding strength. Solvent screening showed that non-coordinating solvents such as toluene and acetonitrile allowed for the deprotection to occur on TiO₂. This is in agreement with our previous assessment that the exposed Ti(IV) atoms or bound acidic water molecules must be accessible and not deactivated by a competing ligand. It is also consistent with our ability to more easily purify the THP-protected products using chromatography on triethylamine-deactivated silica, while degradation occurred in some cases when the parent acidic silica was employed.

Crystalline anatase TiO₂ powder was dispersed into a solution of the sensitizer molecule in anhydrous acetonitrile at various temperatures in order to quantify the surface concentrations of phenyl-HA and phenyl-THP. The surface loading was obtained by measuring the change in concentration of the sensitizer solution after exposure to the particles for a period of 16 h. The results are summarized in Table 1 for

Table 1. TiO₂ Surface Loading for Phenylhydroxamic Acid (Phenyl-HA) and THP-Phenylhydroxamate (Phenyl-THP)

molecule	temp (°C)	loading (molecules·nm ⁻²) ^a
phenyl-HA	22	1.9 ± 0.2
	60	2.0 ± 0.3 ^b
phenyl-THP	22	0.85 ± 0.07
	60	0.95 ± 0.02

^aThe loading was determined by measuring the change in concentration of a 0.3 mM solution of the sensitizer molecule in acetonitrile before and after exposure to dispersed TiO₂ nanoparticles. The average surface area of the nanoparticles as reported by the manufacturer is 50 m²·g⁻¹, which was used to calculate the surface loading. ^bA second species was formed in solution with an absorption peak at ~270 nm in addition to the primary phenyl-HA.

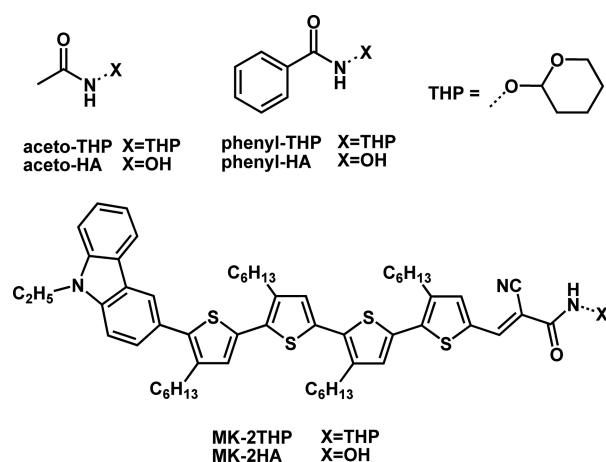


Figure 1. Aceto-, phenyl-, and MK-2 hydroxamate derivatives.

reactions carried out at room temperature and at 60 °C. The loading of the THP-protected species does not display a significant temperature-dependence, which indicates that the surface-mediated deprotection reaction occurs efficiently at room temperature.

In the case of the TiO₂ particles sensitized with phenyl-HA at 60 °C, the peak at 227 nm assigned to the phenyl-HA was accompanied by a second broad peak centered at ~270 nm. Based on recent characterization of solubilized Ti⁴⁺ complexes with phenyl-HA ligands, we assign this peak to the corrosion of the TiO₂ nanoparticles by the phenyl-HA leading to the formation of Ti⁴⁺ complexes in solution during the sensitization.¹⁶ This is consistent with prior reports, which have demonstrated that hydroxamic acid species are utilized by siderophores to solubilize metal atoms.²⁰ This finding further highlights the high binding affinity of hydroxamate anchoring groups to metal oxide surfaces. It is important to note that the

formation of the complex may lead to a slight overestimate of the surface loading since the sensitizer is removed from the solution by both coating the surface of the particles and by forming the complexes in solution.

Interestingly, the loading of the THP-protected species of ~ 0.9 molecules·nm⁻² was less than one-half that of the value of ~ 2 molecules·nm⁻² measured for the free-hydroxamate (Table 1). To investigate this finding further, an NMR study performed in *d*₃-acetonitrile solvent with phenyl-THP and nanoparticulate TiO₂ showed that the entirety of the phenyl-THP molecular components was bound to the surface (Figure S1). The products of the deprotection in a standard solution-phase reaction are the hydroxamic acid and tetrahydro-2H-pyran-2-ol (THP-OH). While this deprotection reaction for THP-hydroxamates is known, the characterization of a heterogeneous metal oxide-catalyzed reaction has not been performed.²¹

To delve deeper into the identity of the surface-bound species, Fourier transform infrared spectra utilizing attenuated total reflectance (FT-IR-ATR) were obtained for TiO₂ functionalized with aceto-HA, aceto-THP, phenyl-HA, phenyl-THP, and THP-OH (Figure 2, with the IR of the

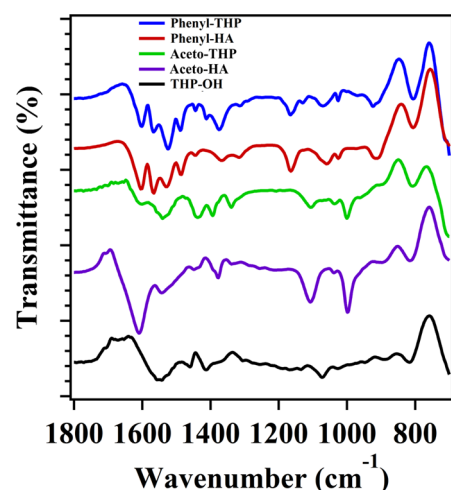


Figure 2. FT-IR-ATR spectra of molecules on anatase TiO₂. Nonfunctionalized TiO₂ was used as background for the experiment. Spectra are vertically offset for clarity, and large *y*-axis tick increments correspond to 1%T.

nonadsorbed compounds shown for comparison in Figure S2). A comprehensive experimental and theoretical analysis of hydroxamate binding to anatase TiO₂ has recently been published by our group,¹⁶ with extensive IR analyses of the surface-bound species. Prominent bands in the range 1450–1600 cm⁻¹ have been attributed to C=O, C–N, and other vibrational modes with strong skeletal coupling causing complicated signals.^{16,22,23} The IR spectra shown in Figure 2 reveal significant overlap for all vibrational peaks between the surface-bound species originating from either the hydroxamic acid or THP analogue, but with an important difference. The aceto- and phenyl-THP analogues show noticeable differences in the spectral range between 1500 and 1600 cm⁻¹ due to an underlying broad peak assigned to the surface-bound byproduct THP-OH. An additional less intense peak near 1400 cm⁻¹ can also be seen. Other THP-OH peaks are generally too broad to be distinguished in the spectrum. Broad inverted peaks related to surface water molecules near 1650 and 775 cm⁻¹ are

characteristic of surface-bound IR spectra of anatase TiO₂ and are the result of displacing surface water molecules with other species.^{16,24}

While we cannot observe the intermediate products of the deprotection prior to surface adsorption, an IR analysis of the unbound hydroxamic acid, THP-protected analogues, and THP-OH (Figure S2) show that numerous bands corresponding to the THP moiety between 800 and 1200 cm⁻¹ disappear when bound to the TiO₂ surface. This is coupled with the rise of the broad band near 1550 cm⁻¹. These are consistent features both for the surface deprotection of THP-protected molecules and the surface-binding of THP-OH. The remaining bands attributed to the surface-bound hydroxamate overlay those of the surface-bound species originating from the pure hydroxamic acid analogue. Thus, the evidence suggests that the products of the surface-mediated deprotection are the hydroxamic acid and THP-OH, both of which bind to TiO₂.

Overall, the IR spectra support the conclusion that the surface connection originating from either the hydroxamic acid or THP analogue is essentially identical and aligns with our NMR-study conclusions that the THP-OH byproduct is also surface-bound in the latter case. Returning to our surface loading studies in Table 1, the evidence suggests that lower surface loading levels from surface-mediated THP deprotection are due to the simultaneous binding of the hydroxamate and the THP-OH species, which decreases the number of active binding sites by increasing the effective molecular footprint.

To extend our study to a practical application, we also examined the surface-mediated deprotection and adsorption of commercially available MK-2 dye functionalized with a THP-protected hydroxamate anchoring group (MK-2THP) on nanoparticulate TiO₂ thin films. We compared these results with the MK-2THP dye that was previously deprotected using standard methods (MK-2HA) before adsorption. In this case, the loading experiments were performed on TiO₂ nanoparticle films immersed into toluene solutions containing MK-2THP or MK-2HA dye, because MK-2 derivatives are not soluble in acetonitrile. In an analogous fashion to the phenyl-THP, the adsorption of MK-2THP in toluene readily occurs at room temperature and the loading did not significantly depend on the adsorption temperature. The TiO₂ surface loadings of the MK-2THP and MK-2HA dyes on TiO₂ nanoparticulate films were determined to be very similar: 63.4 and 66.6 nmol·cm⁻², respectively. This result contrasted with the surface loading of the phenyl-THP and phenyl-HA but is possibly due to the surface coverage being dominated by the relatively large MK-2 dye on the surface compared to the cobound THP-OH. Most of the steric bulk of the MK-2 dye is due to the alkyl chains on the thiophenes, while the dye cross section near the TiO₂ surface is relatively unhindered, possibly allowing the THP-OH to nest in that space between dyes. In addition, the known aggregation of MK-2 analogues could hinder the quantitative analysis.²⁵

We further characterized the binding affinity and aggregation behavior of the MK-2THP and MK-2HA sensitized films by performing dye-desorption studies. Dye desorption was performed in a solution of dimethylformamide (DMF) containing 1% water to facilitate the hydrolysis of the HA–TiO₂ bond, and the concentration of the desorbed dye was measured as a function of time utilizing UV–visible spectroscopy. The resulting desorption curves are shown in Figure 3. The kinetics of dye desorption and the relative mole-fractions of covalently bound dye and nonspecifically bound dye were

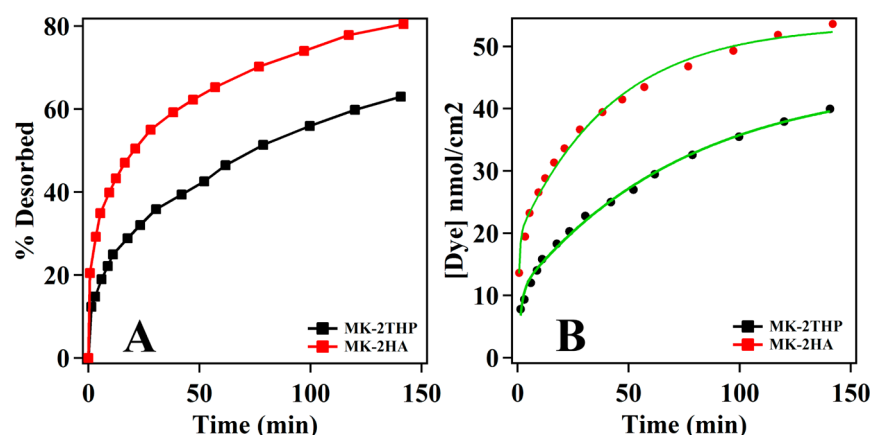


Figure 3. Dye desorption curves shown as the percent dye desorbed (A) and the surface concentration of the dye in nmol/cm^2 (B, normalized to the geometric area of the nanoparticle thin film) as a function of immersion time in a solution of 1% H_2O in DMF. Fits of eq 2 to the experimental data are shown as the green curves.

Table 2. Parameters from Double Exponential Fits of Eq 2 to the Desorption Curves^a

sample	total dye ($\text{nmol}\cdot\text{cm}^{-2}$)	χ_{NS}	k_{NS} (min^{-1})	χ_{CB}	k_{CB} (min^{-1})
MK-2THP	63.4	0.24 ± 0.02	0.7 ± 0.1	0.76 ± 0.04	0.013 ± 0.001
MK-2HA	66.6	0.36 ± 0.01	1.6 ± 0.3	0.64 ± 0.03	0.024 ± 0.002

^aTotal dye was determined using extinction coefficients for MK-2 and the geometric area of the nanoparticulate thin film.

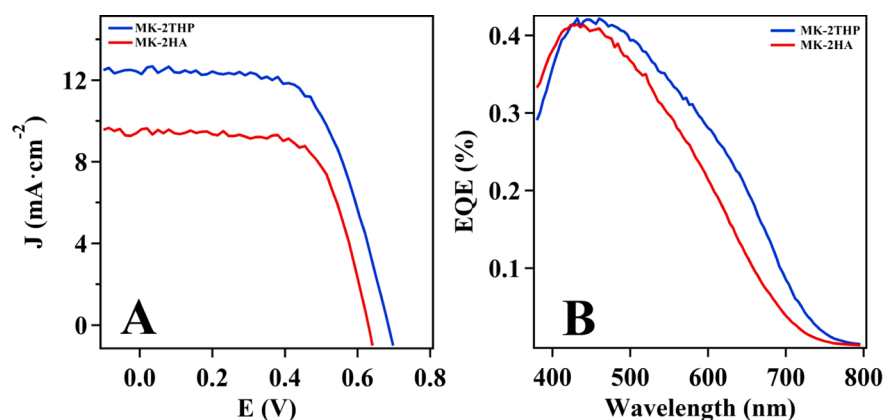


Figure 4. Current density vs applied potential (A) and external quantum efficiency spectra (B) for representative DSPCs sensitized with the MK-2THP and MK-2HA dyes.

determined from fits of the desorption curves (Figure 3B). Previous studies have shown that a monolayer of the MK-2HA dye consists of a combination of dye that is covalently (specifically) bound to the surface and weakly associated dye in the form of aggregated dye particles on the surface of the monolayer.^{12,25,26} In previous reports by our group,^{12,19} the data were fit with a single exponential (eq 1)

$$[\text{dye}]_{\text{soln}} = [\text{dye}]_{\text{total}}\chi_{\text{eq}}(1 - e^{-kt}) + [\text{dye}]_{\text{total}}\chi_{\text{NS}} \quad (1)$$

where $[\text{dye}]_{\text{soln}}$ is the concentration of dye in solution, $[\text{dye}]_{\text{total}}$ is the total concentration of the dye in solution and adsorbed on the particles, k is the desorption rate constant, χ_{eq} is the mole fraction of dye in solution at equilibrium, and χ_{NS} is the mole fraction of dye that is nonspecifically bound to the surface. In this case, it is assumed that the nonspecifically bound dye desorbed instantaneously and is, therefore, treated as an offset to the exponential desorption of the covalently bound dye. Herein, we extend our model and employ a double exponential expression (eq 2)

$$[\text{dye}]_{\text{soln}} = [\text{dye}]_{\text{total}}\chi_{\text{CB}}(1 - e^{-k_{\text{CB}}t}) + [\text{dye}]_{\text{total}}\chi_{\text{NB}}(1 - e^{-k_{\text{NB}}t}) \quad (2)$$

where k_{CB} and χ_{CB} are the rate constant and mole fraction of the covalently bound dye at equilibrium, respectively, and k_{NB} and χ_{NB} are the rate constant and mole fraction of the nonspecifically bound dye in solution at equilibrium, respectively. The results of fitting eq 2 to the data are summarized in Table 2.

In both cases, the nonspecifically bound dye accounts for a significant percentage of the total surface loading and is rapidly desorbed with rate constant $\sim 1 \text{ min}^{-1}$, which is consistent with previous results.¹² The surface-mediated deprotection process leads to a lower fraction of dye aggregation (included in nonspecifically bound desorption data, χ_{NS}) when the surface is loaded with MK-2THP relative to MK-2HA (24% vs 36%). This is consistent with the mechanism of adsorption in the case of the MK-2THP because adsorption can only occur after the THP protecting group is removed by the surface. On the other

hand, adsorption of MK-2HA can proceed rapidly because all of the dye molecules in solution have active hydroxamate anchoring groups.

In terms of the covalently bound dye, the desorption rate constant of the surface-bound MK-2THP is nearly twofold lower than the MK-2HA (0.013 vs 0.024 min⁻¹). In fact, after 150 min of exposure to the desorption solution, Figure 3B reveals that the MK-2THP sensitized film retains 40% of the total dye loading whereas the MK-2HA sensitized film retains only 20%. Collectively, these results suggest that the covalent interaction formed by the surface-mediated deprotection process is less susceptible to hydrolysis than that formed from the free hydroxamic acid. This could be due to the hydrophobic or steric interactions of the cobound THP-OH on the TiO₂. The lower susceptibility to hydrolytic desorption is an added bonus to the already greater stability of hydroxamates over carboxylate linkages, making it even more attractive for applications in aqueous photoelectrochemical cells such as water-splitting cells.²⁷

To investigate the performance of the dye monolayer formed by the surface-mediated deposition process, we assembled operating dye-sensitized photoelectrochemical cells (DSPCs) with films sensitized by the MK-2THP and MK-2HA dyes. The current density vs potential (*J*-*V*) curves (Figure 4A) revealed that the DSPCs sensitized by the surface-mediated deprotection of the MK-2THP led to improved photoelectrochemical performance. The MK-2THP DSPCs maintained an average efficiency of 5.3%, which was significantly enhanced relative to the efficiency of 3.7% measured for the MK-2HA dye (Table 3). The increase in efficiency correlates with increases in the

Table 3. DSPC Characteristics Measured under AM1.5G Light at 100 mW·cm⁻²

DSPC	<i>V</i> _{oc} (V)	<i>J</i> _{sc} (mA·cm ⁻²)	fill factor	efficiency (%)
MK-2THP	0.676 ± 0.008	13 ± 2	0.62 ± 0.03	5.3 ± 0.8
MK-2HA	0.645 ± 0.018	9 ± 2	0.65 ± 0.03	3.7 ± 0.7

short-circuit current density (*J*_{sc}) and the open-circuit voltage (*V*_{oc}) of the MK-2THP DSPC relative to the MK-2HA DSPC. External quantum efficiency (EQE) spectra shown in Figure 4B reveal that the photon to electron conversion efficiency is greater at wavelengths above 450 nm. The increased efficiency at longer wavelengths is likely due to a decrease in light filtering by aggregated dyes, as suggested by our desorption experiments.

The DSPC results demonstrate that the dye monolayer formed by surface-mediated deprotection leads to higher overall photoelectrochemical performance. We suggest that the higher performance results from several advantages of the in situ, surface-mediated deprotection process. First, the surface-mediated process leads to a lower degree of dye aggregation (Table 2), which is consistent with the higher EQE values (Figure 4B). Dye aggregation has been shown previously to result in decreased photon-to-electron conversion efficiency because photoexcited electrons can relax via pathways that do not involve electron injection into the metal oxide surface.²⁶ Second, the desorption results suggest that the surface-mediated process leads to a strong covalent interaction with the surface of the metal oxide, similar to that of the hydroxamic acid analogue. This has been shown in prior studies to lead to

favorable increases in the rate and efficiency of electron transfer.¹⁹

As a preliminary electron-transfer study, the rate of recombination of the charge-separated state was measured by transient absorption of the dye-sensitized TiO₂ films in an acetonitrile solution of 0.1 M NaClO₄. Figure 5 shows the

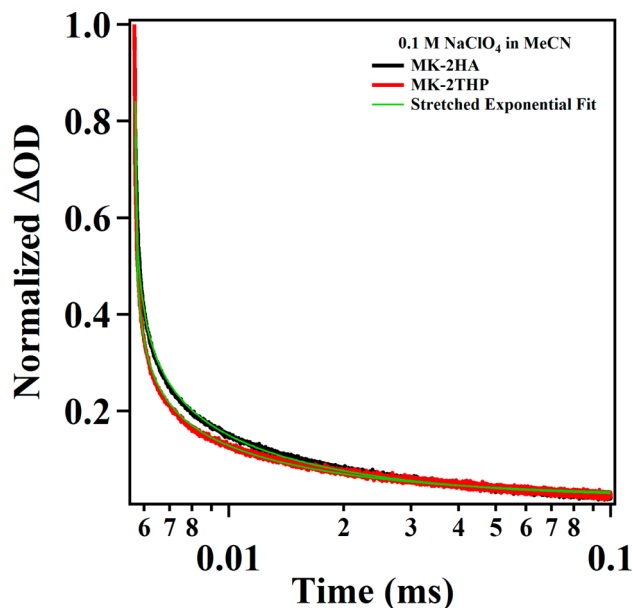


Figure 5. Transient absorption curves measured at 800 nm for the decay of the charge-separated state of MK-2THP and MK-2HA sensitized TiO₂ nanoparticle films immersed in 0.1 M NaClO₄ in acetonitrile. The injection was induced by an optical pump pulse at 560 nm. The green lines depict the stretched exponential curve that was fit to the data.

average transient absorption of the charge-separated state for the MK-2HA and MK-2THP dye. The decay in the transient is associated with the recombination of injected electrons in the conduction band with the oxidized dye. The lifetimes of recombination were determined by fitting a stretched exponential function (eq 3), where *A* is the amplitude, *t* is the time, *t*₀ is the time-offset, *τ* is the lifetime, and *β* is the stretch parameter, which can range from 0 to 1.²⁹

$$\Delta OD_t = A \exp\left(\frac{t - t_0}{\tau}\right)^\beta \quad (3)$$

The average lifetime for the decay of the charge-separated state (*τ*_{ww}) is calculated from the values of *τ* and *β* according to eq 4, where *Γ* is the gamma function.

$$\langle \tau_{ww} \rangle = \frac{\tau}{\beta} \Gamma\left(\frac{1}{\beta}\right) \quad (4)$$

The results of this analysis (Table 4) revealed that the films maintain essentially identical average recombination rates of 3.6

Table 4. Parameters Determined from Fitting a Stretched Exponential Function to the Transients Shown in Figure 5

dye	<i>y</i> ₀	<i>τ</i> (μs)	<i>β</i>	<i>τ</i> _{ww} (μs)
MK-2HA	0.0248(3)	0.36(1)	0.295(6)	3.61
MK-2THP	0.0276(3)	0.189(9)	0.265(6)	3.21

and 3.2 μs . On the basis of these preliminary results, the data suggest that the pathway of electron recombination is similar regardless of how the dye is anchored. Although beyond the scope of this report, time-resolved terahertz spectroscopy experiments are underway to characterize the rate and efficiency of electron injection in these films, both in air and under operating conditions.²⁸

4. CONCLUSIONS

In this study, we have shown that THP-protected hydroxamic acids can act as direct precursors for anchoring to TiO_2 via a surface-mediated reaction. For the molecules with relatively small molecular footprints, this yielded surfaces with decreased coverage density due to cobinding of the THP–OH byproduct. However, the surface coverage obtained for the relatively bulky MK-2THP organic dye is similar to that of the MK-2HA, but with decreased aggregation, causing an increase in DSPC performance. In addition, the surface linkage resulting from surface-mediated deprotection and chelation is more hydrolytically stable than that from the hydroxamic acid. Beyond the ease of synthesis and improved solubility properties of the THP-protected hydroxamates over the hydroxamic acid analogues, they also provide additional benefits in terms of efficiency in photoelectrochemical cells.

The results coincide with our recent analysis of the binding of hydroxamic acids on anatase TiO_2 . The previously determined binding scheme has the hydroxamic acid monodeprotonated and binding in a chelating geometry (Figure 6).¹⁶ The present results show that the surface species

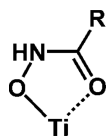


Figure 6. Surface-binding geometry of the hydroxamic acid anchor on TiO_2 where R is an organic substituent.

formed during the surface-mediated THP deprotection were more kinetically stable to hydrolysis than those originating from the hydroxamic acid and suggest that either the former's surface-bonding scheme is different from the latter or the surface itself is different, such as from protective coadsorption of the THP–OH. The similarity of our IR spectroscopic data suggests that the major binding mode for the THP analogues deprotected on TiO_2 is the same as the hydroxamic acid analogues, but this does not take into account either a cooperative effect on the surface with the THP–OH byproduct or reorientation of the surface structure during deprotection as previously suggested.¹⁶ Studies are currently underway to determine the most likely possibilities for the surface-bound geometry.

■ ASSOCIATED CONTENT

Supporting Information

The Supporting Information is available free of charge on the ACS Publications website at DOI: 10.1021/acs.jpcc.6b02635.

Experimental details including the procedure for assembling DSPC devices, ^1H NMR spectra of synthesized compounds, and infrared spectra of reference compounds (PDF)

■ AUTHOR INFORMATION

Corresponding Author

* Email: gary.brudvig@yale.edu; Telephone: +1 (203) 432-5202.

Author Contributions

[§]These authors contributed equally.

Notes

The authors declare no competing financial interest.

■ ACKNOWLEDGMENTS

This work was funded by U.S. Department of Energy Grant DE-FG02-07ER15909 and a generous gift from the TomKat Charitable Trust.

■ REFERENCES

- (1) Young, K. J.; Martini, L. A.; Milot, R. L.; Snoeberger, R. C.; Batista, V. S.; Schmittenmaer, C. A.; Crabtree, R. H.; Brudvig, G. W. Light-Driven Water Oxidation for Solar Fuels. *Coord. Chem. Rev.* **2012**, *256*, 2503–2520.
- (2) Hagfeldt, A.; Boschloo, G.; Sun, L.; Pettersson, H. Dye-Sensitized Solar Cells. *Chem. Rev.* **2010**, *110*, 6595–6663.
- (3) Galoppini, E. Linkers for Anchoring Sensitizers to Semiconductor Nanoparticles. *Coord. Chem. Rev.* **2004**, *248*, 1283–1297.
- (4) Oh, S. J.; Cho, S. J.; Kim, C. O.; Park, J. W. Characteristics of DNA Microarrays Fabricated on Various Aminosilane Layers. *Langmuir* **2002**, *18*, 1764–1769.
- (5) Vlassiounk, I.; Park, C.-D.; Vail, S. A.; Gust, D.; Smirnov, S. Control of Nanopore Wetting by a Photochromic Spiropyran: A Light-Controlled Valve and Electrical Switch. *Nano Lett.* **2006**, *6*, 1013–1017.
- (6) Blumenfeld, C. M.; Grubbs, R. H.; Moats, R. A.; Gray, H. B.; Sorasaene, K. Decorating Metal Oxide Surfaces with Fluorescent Chlorosulfonated Corroles. *Inorg. Chem.* **2013**, *52*, 4774–4776.
- (7) McNamara, W. R.; Milot, R. L.; Song, H.-e.; Snoeberger, R. C., III; Batista, V. S.; Schmittenmaer, C. A.; Brudvig, G. W.; Crabtree, R. H. Water-Stable, Hydroxamate Anchors for Functionalization of TiO_2 Surfaces with Ultrafast Interfacial Electron Transfer. *Energy Environ. Sci.* **2010**, *3*, 917–923.
- (8) McNamara, W. R.; Snoeberger, R. C., III; Li, G.; Richter, C.; Allen, L. J.; Milot, R. L.; Schmittenmaer, C. A.; Crabtree, R. H.; Brudvig, G. W.; Batista, V. S. Hydroxamate Anchors for Water-Stable Attachment to TiO_2 Nanoparticles. *Energy Environ. Sci.* **2009**, *2*, 1173–1175.
- (9) Martini, L. A.; Moore, G. F.; Milot, R. L.; Cai, L. Z.; Sheehan, S. W.; Schmittenmaer, C. A.; Brudvig, G. W.; Crabtree, R. H. Modular Assembly of High-Potential Zinc Porphyrin Photosensitizers Attached to TiO_2 with a Series of Anchoring Groups. *J. Phys. Chem. C* **2013**, *117*, 14526–14533.
- (10) Brennan, B. J.; Keirstead, A. E.; Liddell, P. A.; Vail, S. A.; Moore, T. A.; Moore, A. L.; Gust, D. 1-(3'-Amino)Propylsilatrane Derivatives as Covalent Surface Linkers to Nanoparticulate Metal Oxide Films for Use in Photoelectrochemical Cells. *Nanotechnology* **2009**, *20*, 505203.
- (11) Brewster, T. P.; Konezny, S. J.; Sheehan, S. W.; Martini, L. A.; Schmittenmaer, C. A.; Batista, V. S.; Crabtree, R. H. Hydroxamate Anchors for Improved Photoconversion in Dye-Sensitized Solar Cells. *Inorg. Chem.* **2013**, *52*, 6752–6764.
- (12) Koenigsmann, C.; et al. Substitution of a Hydroxamic Acid Anchor into the MK-2 Dye for Enhanced Photovoltaic Performance and Water Stability in a DSSC. *Phys. Chem. Chem. Phys.* **2014**, *16*, 16629–16641.
- (13) Materna, K. L.; Brennan, B. J.; Brudvig, G. W. Silatrane for Binding Inorganic Complexes to Metal Oxide Surfaces. *Dalton Trans* **2015**, *44*, 20312–5.
- (14) Brennan, B. J.; Llansola Portoles, M. J.; Liddell, P. A.; Moore, T. A.; Moore, A. L.; Gust, D. Comparison of Silatrane, Phosphonic Acid, and Carboxylic Acid Functional Groups for Attachment of Porphyrin

Sensitizers to TiO₂ in Photoelectrochemical Cells. *Phys. Chem. Chem. Phys.* **2013**, *15*, 16605–14.

(15) Kryman, M. W.; Nasca, J. N.; Watson, D. F.; Detty, M. R. Selenorhodamine Dye-Sensitized Solar Cells: Influence of Structure and Surface-Anchoring Mode on Aggregation, Persistence, and Photoelectrochemical Performance. *Langmuir* **2016**, *32*, 1521–1532.

(16) Brennan, B. J.; Chen, J.; Rudshiteyn, B.; Chaudhuri, S.; Mercado, B. Q.; Batista, V. S.; Crabtree, R. H.; Brudvig, G. W. Molecular Titanium–Hydroxamate Complexes as Models for TiO₂ Surface Binding. *Chem. Commun.* **2016**, *52*, 2972–2975.

(17) Sartori, G.; Maggi, R. Update 1 Of: Protection (and Deprotection) of Functional Groups in Organic Synthesis by Heterogeneous Catalysis. *Chem. Rev.* **2010**, *110*, PR1–PR54.

(18) Li, C.; Koenigsmann, C.; Deng, F.; Hagstrom, A.; Schmuttenmaer, C. A.; Kim, J.-H. Photocurrent Enhancement from Solid-State Triplet–Triplet Annihilation Upconversion of Low-Intensity, Low-Energy Photons. *ACS Photonics* **2016**, *3*, 784.

(19) Li, C.; et al. Facet-Dependent Photoelectrochemical Performance of TiO₂ Nanostructures: An Experimental and Computational Study. *J. Am. Chem. Soc.* **2015**, *137*, 1520–1529.

(20) Miller, M. J. Syntheses and Therapeutic Potential of Hydroxamic Acid Based Siderophores and Analogs. *Chem. Rev.* **1989**, *89*, 1563–1579.

(21) Misra, R. N.; Botti, C. M.; Haslanger, M. F.; Engebrecht, J. R.; Mahoney, E. M.; Ciosek, C. P. Cyclic Aryl Hydroxamic Acids: Synthesis and Inhibition of 5-Lipoxygenase. *Bioorg. Med. Chem. Lett.* **1991**, *1*, 295–298.

(22) Yang, J.; Bremer, P. J.; Lamont, I. L.; McQuillan, A. J. Infrared Spectroscopic Studies of Siderophore-Related Hydroxamic Acid Ligands Adsorbed on Titanium Dioxide. *Langmuir* **2006**, *22*, 10109–10117.

(23) Li, W.; Rego, L. G. C.; Bai, F.-Q.; Kong, C.-P.; Zhang, H.-X. Theoretical Investigation of the Adsorption, IR, and Electron Injection of Hydroxamate Anchor at the TiO₂ Anatase (101) Surface. *RSC Adv.* **2014**, *4*, 19690–19693.

(24) Capecci, G.; Faga, M. G.; Martra, G.; Coluccia, S.; Iozzi, M. F.; Cossi, M. Adsorption of CH₃COOH on TiO₂: IR and Theoretical Investigations. *Res. Chem. Intermed.* **2007**, *33*, 269–284.

(25) Nepomnyashchii, A. B.; Parkinson, B. A. Influence of the Aggregation of a Carbazole Thiophene Cyanoacrylate Sensitizer on Sensitized Photocurrents on ZnO Single Crystals. *Langmuir* **2013**, *29*, 9362–9368.

(26) Wang, Z.-S.; Koumura, N.; Cui, Y.; Takahashi, M.; Sekiguchi, H.; Mori, A.; Kubo, T.; Furube, A.; Hara, K. Hexylthiophene-Functionalized Carbazole Dyes for Efficient Molecular Photovoltaics: Tuning of Solar-Cell Performance by Structural Modification. *Chem. Mater.* **2008**, *20*, 3993–4003.

(27) Moore, G. F.; Blakemore, J. D.; Milot, R. L.; Hull, J. F.; Song, H.; Cai, L.; Schmuttenmaer, C. A.; Crabtree, R. H.; Brudvig, G. W. A Visible Light Water-Splitting Cell with a Photoanode Formed by Codeposition of a High-Potential Porphyrin and an Iridium Water-Oxidation Catalyst. *Energy Environ. Sci.* **2011**, *4*, 2389–2392.

(28) Nemes, C. T.; Koenigsmann, C.; Schmuttenmaer, C. A. Functioning Photoelectrochemical Devices Studied with Time-Resolved Terahertz Spectroscopy. *J. Phys. Chem. Lett.* **2015**, *6*, 3257–3262.

(29) Abrahamsson, M.; Johansson, P. G.; Ardo, S.; Kopecky, A.; Galoppini, E.; Meyer, G. J. Decreased Interfacial Charge Recombination Rate Constants with N3-Type Sensitizers. *J. Phys. Chem. Lett.* **2010**, *1*, 1725–1728.

Supporting Information

Surface-Induced Deprotection of THP-Protected Hydroxamic Acids on Titanium Dioxide

Bradley J. Brennan,[†] Christopher Koenigsmann,[‡] Kelly L. Materna,[†] Paul M. Kim,[†] Matthieu Koepf,[†] Robert H. Crabtree,[†] Charles A. Schmuttenmaer,[†] and Gary W. Brudvig^{†*}

[†]Energy Sciences Institute and Department of Chemistry, Yale University, P.O. Box 208107, New Haven, Connecticut 06520-8107

[‡]Department of Chemistry, Fordham University, 441 East Fordham Road, Bronx, NY 10458

* E-mail: gary.brudvig@yale.edu

Supporting Information Contents:

Assembly of Dye Sensitized Photoelectrochemical Cell (DSPCs).....	S2
Nanosecond transient absorption	S2
Figure S1. ¹ H NMR in d ₃ -acetonitrile of Phenyl-THP	S3
Figure S2. FT-IR-ATR spectra	S4
References.....	S5

Assembly of Dye Sensitized Photoelectrochemical Cell (DSPCs)

Photoanodes were prepared on TEC15 FTO glass (Hartford Glass).¹⁻² The TEC15 glass was pretreated with a compact TiO₂ thin film by immersing the glass into an aqueous solution of 40 mM titanium chloride at 75 °C for a period of 30 min. The TiO₂ film was crystallized by annealing at 570 °C for a period of 10 min. A mesoporous TiO₂ film consisting of 15 µm transparent TiO₂ nanoparticles (Solaronix, T/SP) and 10 µm scattering TiO₂ (Dyesol, 18NR-AO) was deposited by doctor-blading. The films were crystallized at 470 °C for a period of 30 min. Finally, the FTO and mesoporous film were treated a second time with the titanium chloride solution and the substrate was re-annealed at 570 °C for 10 min. Thin films of mesoporous TiO₂ for FTIR studies were prepared by diluting the transparent paste with a mixture consisting of 50% α -terpineol and 50% of an ethyl cellulose solution prepared in ethanol.

Solutions of the sensitizers were prepared in either anhydrous acetonitrile (Phenyl-THP & Phenyl-HA) or anhydrous toluene (MK-2THP & MK-2HA) with a concentration of ~0.3 mM. While still hot (~80 °C) from the final annealing process, the films were transferred into the sensitizer solutions and allowed to sensitize for a period of 16 h. In the experiments with sensitization performed at elevated temperatures, the sensitizer solution was pre-heated under argon to the desired temperature before adding the mesoporous TiO₂ film. In all cases, the films were simultaneously sensitized with the hydroxamic acid and THP-protected hydroxamic acid under identical conditions (*i.e.* in the same heating bath) to avoid any variation in the time or temperature from sample-to-sample.

The counter electrodes were prepared on TEC7 FTO pieces (Hartford Glass) and a 1 mm hole was pre-drilled to allow for the introduction of electrolyte. A solution of 8 wt% hexachloroplatinic acid was brushed onto the surface and allowed to dry under ambient conditions. The platinum was crystallized by heating the substrates at 450 °C for 30 min. Functioning devices were assembled by bonding the photoanode with the cathode using a 60 µm thick Surelyn heat melt spacer. The electrolyte was introduced into the cell by vacuum backing filling. In this case, the electrolyte consisted of combination of 1,2-dimethyl-3-propylimidazolium iodide (DMPII, TCI, 0.6 M), lithium iodide (anhydrous, 99.95%, Alfa Aesar, 0.1 M), iodine (pure, Acros Organics, 0.2 M), 4-*tert*-butylpyridine (TBP, Sigma-Aldrich, 0.5 M) and anhydrous acetonitrile as the solvent (Omni Solv, EMD Millipore).

Nanosecond transient absorption

Transient absorption measurements were performed with a LP920 laser flash photolysis spectrometer (Edinburgh Instruments). Excitation of the sample achieved using an optical parametric oscillator (OPO, Spectra-Physics basiScan-M, 1 cm beam diameter, 200 mJ per pulse), pumped by the third harmonic of a Nd:YAG laser system (Spectra-Physics Quanta-Ray INDI 40-10, 5 – 8 ns pulses, operated at 1 Hz). The output of the OPO produced a pulse with a wavelength of 560 nm. A combination of short- and long-pass filters placed between the sample and the detector removed scattered light from the laser pulse. The white light probe was produced by a 450 W Xe arc lamp pulsed at 1 Hz. Transmitted light was focused into a 0.3 m focal length monochromator and was detected by a photomultiplier tube (PMT, Hamamatsu, LP920-K Near-IR detector). Single wavelength transient absorption curves were collected at 800 nm. The PMT current was amplified and recorded with a transient digitizer (Tektronix TDS 3032C). The samples consisted of TiO₂ films deposited onto TEC 15 FTO glass, which were

sensitized with the appropriate dye. The films were placed into a 1 cm × 1 cm quartz cuvette at a 45° angle containing 0.1 M NaClO₄ in acetonitrile.

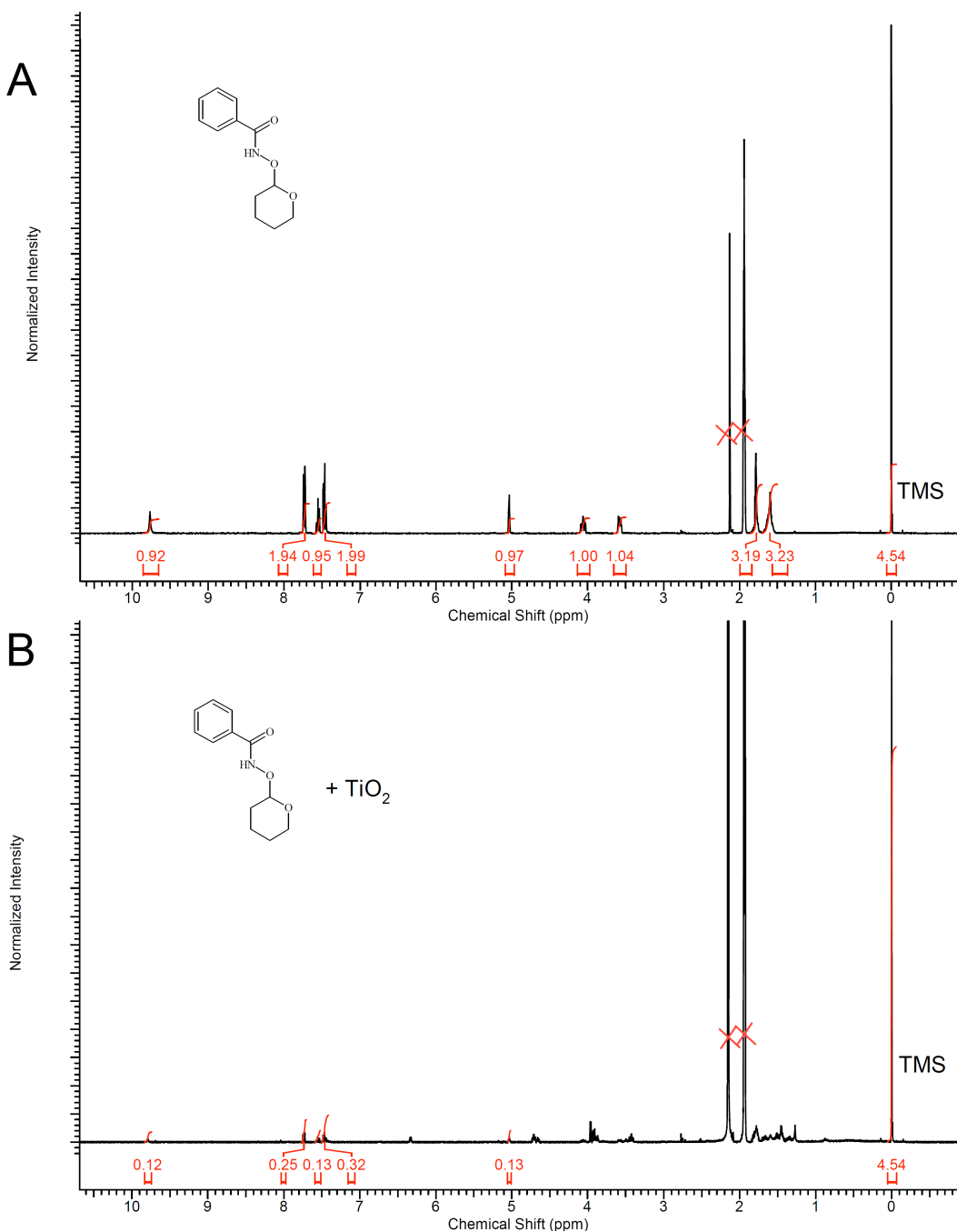


Figure S1. ¹H NMR in d₃-acetonitrile of Phenyl-THP before (A) and soaking overnight at room temperature with anatase TiO₂ powder (B). Tetramethylsilane was used as internal standard for integration. Signals for acetonitrile and water show increased signals, likely due to proton exchange with the TiO₂ surface water monolayer. Residual signals for Phenyl-THP are highlighted for integration purposes, but minor impurities or detritus from unknown decompositions overlay peaks for the THP moiety.

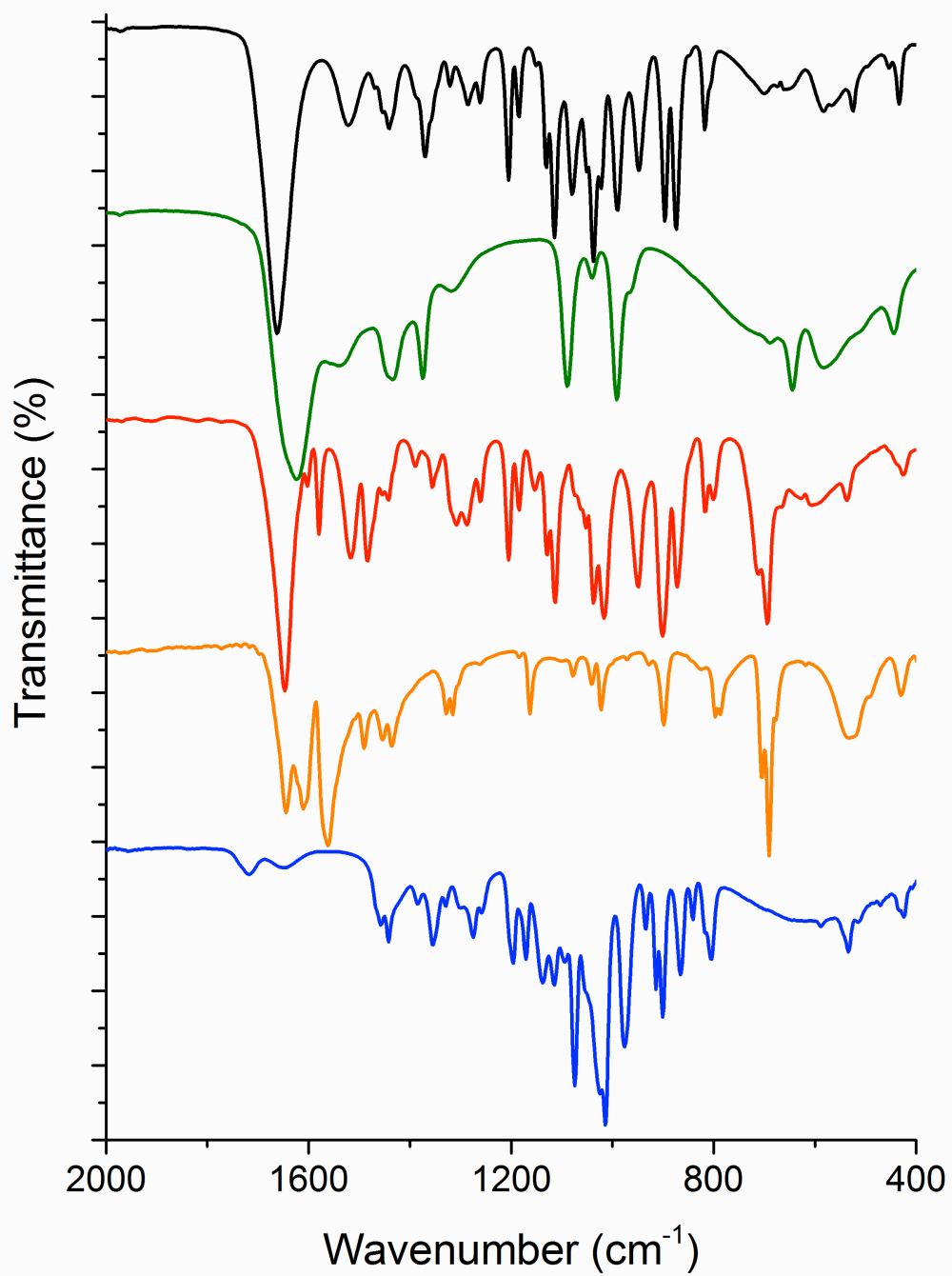


Figure S2. FT-IR-ATR spectra of pure aceto-THP (black), aceto-HA (green), phenyl-THP (red), phenyl-HA (orange), and THP-OH (blue).

References

1. Li, C., et al., Facet-Dependent Photoelectrochemical Performance of TiO₂ Nanostructures: An Experimental and Computational Study. *J. Am. Chem. Soc.* **2015**, *137*, 1520-1529.
2. Brewster, T. P.; Konezny, S. J.; Sheehan, S. W.; Martini, L. A.; Schmuttenmaer, C. A.; Batista, V. S.; Crabtree, R. H., Hydroxamate Anchors for Improved Photoconversion in Dye-Sensitized Solar Cells. *Inorg. Chem.* **2013**, *52*, 6752-6764.